Transonic Separated Flow Predictions with an Eddy-Viscosity/Reynolds-Stress Closure Model

D. A. Johnson*
NASA Ames Research Center, Moffett Field California

In previous work, a new turbulence-closure model was specifically developed for two-dimensional, turbulent boundary layers subjected to strong, adverse-pressure gradients and the attendant separation. This closure model was shown to perform well, but the inverse, boundary-layer calculations used in evaluating the model were not truly predictive since the mass-flux parameter distribution obtained from the experimental data had to be specified. The objective of this study was to evaluate this closure model for a series of strong, transonic, inviscid-viscous interactions with varying degrees of separation using a fully predictive calculation method based on the Reynolds-averaged, Navier-Stokes equations. Calculated results are compared with experimental results and are shown to be in excellent agreement, even for the interactions with massive separation. This closure model has the very favorable property of requiring little more computational effort than equilibrium, algebraic models.

Introduction

SINCE the development of time-marching, Reynolds-averaged, Navier-Stokes methods, considerable attention has been focused on applying them to compressible aerodynamic flow problems with the goal of accurately describing viscous effects at high Reynolds numbers. A major thrust of the research has been in the application of these methods to the aerodynamically important transonic regime.

Because of the ellipticity of transonic flows, the accurate prediction of surface pressure can be extremely difficult when the interaction between the inviscid and viscous flow regions is strong. Unlike supersonic flows, where the shock wave location is strongly controlled by geometry, the resultant shock location and surface pressure distribution in transonic flows can be drastically affected by the viscous-flow development. This is especially true when the inviscid-viscous interaction is strong enough to cause extensive separation. Such cases represent a severe test for any turbulence-closure model used in the Reynolds-averaged, Navier-Stokes equations. In Ref. 1, for example, rather poor predictions of surface pressure were obtained for transonic, inviscid-viscous interactions of varying strength (all developed some separation) with both the Cebeci-Smith, an algebraic, eddy-viscosity model, and the Jones-Launder, a two-equation, eddy-viscosity model.

Recently, a mathematically simple closure model was proposed which shows promise in treating the wall-bounded shear flows that develop in strong, inviscid-viscous interactions.[2] This paper is a further evaluation of this closure model, which is based on a single, ordinary differential equation. Reference 2 presents preliminary evaluations made of this closure model using an inverse-boundary-layer method. However, the calculations were not truly predictive since the mass-flux parameter ($\rho_e u_e \delta^*$) of the experiments had to be specified. The objective of this study was to evaluate the performance of this closure model using a fully predictive numerical calculation procedure. To do this, the closure model was incorporated into a computer code based on MacCormack's semi-implicit, Navier-Stokes algorithm.[3]

The strong, transonic, inviscid-viscous interactions generated on the axisymmetric-bump model of Ref. 4 were selected for the evaluations. The turbulent Reynolds stresses, as well as the mean-velocity field, were measured in this experiment, making it ideal for closure-model evaluations. Also, previous calculations[1] had been peformed based on other turbulence closure models, so that relative performance assessments could be made.

Experiment

The wind-tunnel test model of Ref. 4 consists of a thin-walled cylinder (15.2-cm o.d.), with an axisymmetric, circular-arc bump attached 61 cm from the cylinder leading edge. The bump has a thickness of 1.9 cm and a chord length of 20.3 cm. This flow model was designed specifically to simulate the type of inviscid-viscous interactions which can develop on airfoil sections at transonic conditions. An axisymmetric configuration was selected to minimize wind-tunnel wall effects and to insure maintenance of two-dimensionality even under conditions of massive separation. That the wind-tunnel walls had, at most, a very small effect on the flow developed around this model was demonstrated through tests conducted in two facilities that differed significantly in size; the Ames 2×2-ft Transonic Wind Tunnel and the Ames 6×6-ft Supersonic Wind Tunnel. In Fig. 1, surface-pressure distributions obtained in these two wind tunnels at a freestream Mach number of 0.875 and a unit Reynolds number of $10(10)^6$/m are compared. A sketch of the wind tunnel is included in this figure.

Computations

The same computer program used in Ref. 1, which is based on the semi-implicit algorithm of MacCormack,[3] was used in this study. The boundary conditions, as in Ref. 1, were as follows:

1) At the upstream boundary, uniform, freestream conditions were presecribed holding total pressure constant.

2) At the downstream boundary, all gradients in the flow direction were set to zero.

3) No-slip conditions were applied at the model surface, along with a set, constant wall temperature.

Presented as Paper 85-1683 at the AIAA 18th Fluid Dynamics, Plasmadynamics and Lasers Conference, Cincinnati, OH, July 16–18, 1985; received Sept. 17, 1985; revision received June 27, 1986.

*Research Scientist. Member AIAA.

4) At the outer boundary, uniform freestream conditions were used.

The computational domain extended in the flow direction from -140 to 90 cm. ($x=0$ corresponds to the leading edge of circular-arc section.) The upper freestream boundary was located 75 cm from the model surface. A 129×45 mesh was used with a variable point spacing in both coordinate directions. In the streamwise direction, mesh spacing varied from 0.16 cm ($\Delta x/c=0.008$) in the shock region to 12 cm ($\Delta x/c=0.59$) at the downstream boundary. The boundary-layer thickness and displacement thickness just upstream of the shock were 0.81 and 0.13 cm, respectively. Downstream of the circular-arc section, the wind-tunnel model was approximated as a constant-diameter cylinder. This computational mesh, as briefly described, was the same as that used in Ref. 1.

Initially, the same y mesh, with $y^+_{\min}\cong0.8$, was used, as in the previous Jones-Launder model calculations. Then, since this model did not require grid points as near to the surface, a new y-grid spacing was selected with the minimum wall coordinate, $y^+_{\min}\cong2.5$, to reduce solution times. Solutions obtained with the two different y spacings were found to be nearly identical.

Present Closure Model

The closure model discussed in Ref. 2 can best be described as a hybrid eddy-viscosity/Reynolds-shear-stress-model. To account for the strong "history effects" present in flows with large and rapidly changing streamwise pressure gradients, a simplified Reynolds-shear-stress equation (an ordinary differential equation for the maximum Reynolds shear stress) is used to determine eddy-viscosity changes in the streamwise direction. A tendency of eddy-viscosity models is to predict too rapid a change in the Reynolds shear stress when the mean flowfield is suddenly distorted. The subject closure model prevents this from happening by insuring that a rate equation for the maximum Reynolds shear stress is satisfied, regardless of how rapidly to the flow is distorted. A description of this closure model and how it was incorporated into the time-marching, Navier-Stokes method of Ref. 3 follows.

The turbulent eddy viscosity ν_t is assumed to have the functional form

$$\nu_t=\nu_{to}(1-\exp-\nu_{ti}/\nu_{to}) \tag{1}$$

where ν_{ti} and ν_{to} are given by the following:

$$\nu_{ti}=D^2\kappa y(-\overline{u'v'_m})^{1/2} \tag{2}$$

$$\nu_{to}=\sigma(x)\cdot(0.0168u_e\delta_i^*\gamma) \tag{3}$$

A value of 0.4 is assumed for the Kármán constant κ in Eq. (2). The modeling parameter $\sigma(x)$ in Eq. (3) is an unknown that varies with streamwise distance. As will be described later, $\sigma(x)$ is determined by solving an ordinary differential equation for the maximum Reynolds shear stress. In Eq. (3), γ is Klebanoff's intermittency function $\{\gamma=1/[1+5.5\times(y/\delta)^6]\}$.

In Eq. (2), the maximum Reynolds shear stress divided by the local density $-\overline{u'v'_m}$ is taken to be the value determined from the previous time step. (For convenience, $-\overline{u'v'}$ will be referred to as the Reynolds shear stress in this paper.) Notice that Eq. (2) differs from the mixing-length formulation normally used in algebraic, eddy-viscosity models.

The solutions presented in this paper were obtained using the following expression for the near-wall damping term D in Eq. (2):

$$D=1-\exp-(-\overline{u'v'_m})^{1/2}y/\nu A^+ \tag{4}$$

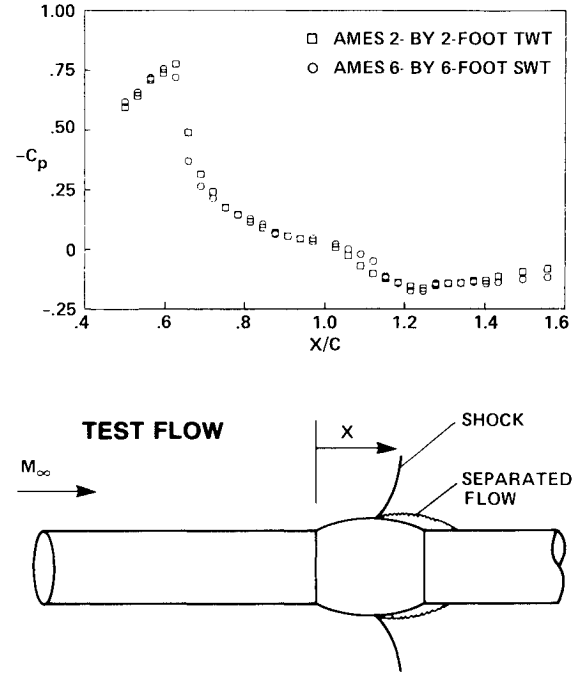

Fig. 1 Comparison of measured surface-pressure distributions at $M_\infty=0.875$ and $Re/m=10(10)^6$.

where $A^+=15$. A value of 15 for A^+ is used instead of the usual value of 26 because of the y^3-dependency of Eq. (2) in the near-wall region. (Mixing-length formulations have a y^4-dependency.) For the flows considered in this paper, nearly identical predictions of surface pressure and viscous-layer growth were obtained when the damping expression of the Cebeci-Smith model (but with $A^+=15$) was used instead of Eq. (4). However, in airfoil calculations,[5] the Cebeci-Smith damping expression yielded unsteady solutions, whereas steady solutions were obtained when Eq. (4) was used. This was also observed in the supersonic, compression-corner calculations of Ref. 6.

The ordinary differential equation used to describe the streamwise development of the maximum Reynolds shear stress is given by

$$(-\overline{u'v'_m})^{1/2}=(-\overline{u'v'_{\rm eq}}|_m)^{1/2}-\underbrace{\frac{L_m\bar{u}_m}{a_1(-\overline{u'v'_m})}\frac{\mathrm{d}(-\overline{u'v'_m})}{\mathrm{d}x}}_{\text{contribution from convection}}$$

$$\underbrace{-\frac{L_m}{(-\overline{u'v'_m})}\mathfrak{D}_m}_{\text{contribution from diffusion}} \tag{5}$$

The subscript m and the vertical slash m denote that the quantity is evaluated at y_m, the y location where $-\overline{u'v'}$ is a maximum. This ordinary differential equation is a simplification of the shear-stress, partial-differential equation of Bradshaw et al.[7] It has been employed in the formulation of integral boundary-layer method by McDonald[8] and Green et al.[9] but is not used directly in those methods. In the former method, it is used to obtain an expression for the shear-stress integral and, in the latter method, to obtain an expression for the entrainment coefficient.

In Eq. (5), L_m is the dissipation length scale, a_1 the ratio of Reynolds shear stress to the turbulence kinetic energy, $\mathfrak{D}_m$ the turbulent diffusion, and $-\overline{u'v'_{\rm eq}}|_m$ the resultant maximum Reynolds shear stress when convection and diffusion effects are negligibly small. This latter quantitity is deter-

mined from Eqs. (1-3), with $\sigma(x)$ in Eq. (3) set equal to unity and $-\overline{u'v'_m}$ in Eq. (2) replaced by $-\overline{u'v'_{eq}}|_m$. Values for L_m and $\mathfrak{D}_m$ are given by the following:

$$L_m = 0.4y_m, \qquad y_m/\delta \leq 0.225 \tag{6a}$$

$$L_m = 0.09\delta, \qquad y_m/\delta > 0.225 \tag{6b}$$

$$\mathfrak{D}_m = \frac{C_{dif}(-\overline{u'v'_m})^{1/2}}{a_1\delta[0.7-(y/\delta)_m]}\,|1-\sigma(x)^{1/2}| \tag{7}$$

The term C_{dif} in Eq. (7) is a modeling constant. The turbulent diffusion term in Eq. (5) is most important in regions where $-\overline{u'v'_m}$ is decreasing with streamwise distance. It has been observed that the neglect of the turbulent diffusion in Eq. (5) results in the prediction of much too slow a decay rate in $-\overline{u'v'_m}$. At the other extreme, a bound on the maximum possible decay rate of $-\overline{u'v'_m}$ can be obtained by assuming that, in regions of decreasing $-\overline{u'v'_m}$, the turbulent diffusion is so large that it balances the convective term in Eq. (5). Under this assumption, Eq. (5) reduces simple to $-\overline{u'v'_m} = -\overline{u'v'_{eq}}|_m$. As described in the "Results" section, solutions were obtained based on both the application of Eq. (7) and this latter simplifying assumption. As in Ref. 2, values of 0.25 and 0.5 were used for the modeling constants a_1 and C_{dif}, respectively.

The unknown $\sigma(x)$ in Eq. (3) provides the link between the assumed algebraic, eddy-viscosity distribution of Eqs. (1-3) and the rate equation for the streamwise development of the maximum Reynolds shear stress of Eq. (5). Through iteration, a $\sigma(x)$ distribution is established, wherein $-\overline{u'v'_m}$ given by

$$-\overline{u'v'_m} = \nu_t\Big|_m\left(\frac{\partial\bar{u}}{\partial y}+\frac{\partial\bar{v}}{\partial x}\right)\Big|_m \tag{8}$$

coincides with the $-\overline{u'v'_m}$ determined from Eq. (5). More specifically, at each time advance, two values of $-\overline{u'v'_m}$ were determined: one based on the eddy-viscosity distribution given by Eqs. (1-3) and the computed mean velocities, and the other based on the integration of Eq. (5). [This equation was integrated using the implicit Euler method after linearization by the variable change, $g=(-\overline{u'v'_m})^{-1/2}$.] Associated with the former $-\overline{u'v'_m}$ are the eddy viscosities $\nu_t|_m$, $\nu_{ti}|_m$, and $\nu_{to}|_m$ and the strain rate

$$\left(\frac{\partial\bar{u}}{\partial y}+\frac{\partial\bar{v}}{\partial x}\right)\Big|_m$$

A pseudo-eddy-viscosity $\tilde{\nu}_t|_m$ was calculated using this strain rate and the $-\overline{u'v'_m}$ obtained from Eq. (5). These four eddy viscosities, $\nu_t|_m$, $\nu_{ti}|_m$, $\nu_{to}|_m$, and $\tilde{\nu}_t|_m$, were used to establish an updated value for $\sigma(x)$ as follows. Two iterations ($n=1$ and 2) of the following algorithm were applied:

$$\nu_{to}|_m^{(n+1)} = \nu_{to}|_m^{(n)}\,\frac{\tilde{\nu}_t|_m}{\nu_t|_m^{(n)}} \tag{9}$$

$$\nu_t|_n^{(n+1)} = \nu_{to}|_m^{(n+1)}\,[1-\exp-\nu_{ti}|_m/\nu_{to}|_m^{(n+1)}] \tag{10}$$

with the update for $\sigma(x)$ given by

$$\sigma(x) = \sigma(x)\,\frac{\nu_{to}|_m^{(3)}}{\nu_{to}|_m^{(1)}} \tag{11}$$

The superscripts in these equations are iteration levels, not exponents, and the lack of an exponent means that the quantity retains its original value. Equation (9) was obtained form Newton's formula by approximating $\partial\nu_t/\partial\nu_{to}$ by $1-\exp-\nu_{ti}/\nu_{to}$.

Solutions based on this closure model were obtained as follows. Starting from a Cebeci-Smith model converged solution, the eddy-viscosity distribution, given by Eqs. (1-3) with $\sigma(x)$ set equal to unity, was imposed at all stations downstream of a specified streamwise station. Once a converged solution was obtained with this eddy-viscosity distribution, $\sigma(x)$ was allowed to change according to Eq. (11) to obtain a final solution. Subsequent solutions for other freestream conditions were obtained starting from converged solutions based on the subject-closure model with all of the flow variables scaled by the new freestream values. In all of the solutions, the Cebeci-Smith model was used to predict Reynolds shear stresses upstream of $x/c=-1$.

Results

In the results to be presented (unless noted otherwise), $\sigma(x)$ was not allowed to exceed unity in the vicinity and downstream of flow reattachment. A solution for $M_\infty = 0.875$ was first obtained with Eq. (7) applied throughout the flowfield but $\sigma(x)$ was observed to reach levels in the flow reattachment region which were excessively high. In fact, an upper bound of 4.0 was imposed on $\sigma(x)$, and that bound had to be applied between $x/c=1.3$ and 1.6. In that interval, Eq. (5) was not satisfied. Since limiting $\sigma(x)$ to a

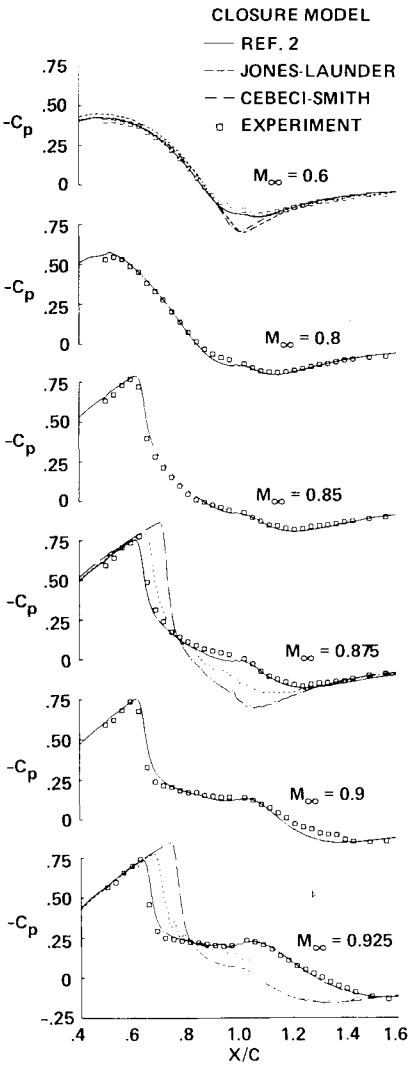

Fig. 2 Comparison of predicted and experimental surface-pressure distributions for a series of freestream Mach numbers.

value of unity in this region was found to have only a minimal effect on the solutions, it was decided to invoke this condition in the subsequent calculations. Only a slight reduction in the boundary-layer recovery rate downstream of reattachment (with no discernible change in the surface-pressure distribution) resulted when $\sigma(x)$ was not allowed to exceed unity. The excessively large values of $\sigma(x)$ which resulted when Eq. (7) was invoked in this region were caused by the underestimation by Eq. (2) of the eddy viscosity in the inner part of the boundary layer, rather than the prediction of too slow a decay rate in $-\overline{u'v'_m}$ by Eq. (5). This will be discussed in more detail in the next section.

The computed, surface-pressure distributions, based on the closure model of Ref. 2 with the turbulent diffusion treated in the manner just described, are compared to the experimental results for freestream Mach numbers ranging from 0.6 to 0.925 in Fig. 2. Included in this figure are the results obtained in Ref. 1 at $M_\infty = 0.6$, 0.875, and 0.925 only, with the Cebeci-Smith[10] and Jones-Launder[11] closure models. In the Jones-Launder model calculations, the longitudinal curvature correction of Ref. 12 was applied, and solutions were obtained by integration to the wall. Except for the $M_\infty = 0.875$ case, the data presented are from the Ames 6×6-ft Supersonic Wind Tunnel. The calculations and the experimental data from the 6×6-ft Supersonic Wind Tunnel are for a unit Reynolds number of $10(10)^6$/m, whereas the data from the 2×2-ft Wind Tunnel are for a unit Reynolds number of $13(10)^6$/m. But, at $M_\infty = 0.875$, solutions were obtained for both of these Reynolds numbers and were essentially identical. Overall, the predicted surface-pressure distributions, based on the closure model of Ref. 2, agree quite well with the experimental results. The predictions are clearly superior to those obtained with either the Cebeci-Smith or Jones-Launder closure models.

An examination of the boundary-layer displacement thickness distributions reveals that the calculated, surface-pressure distributions, as expected, are closely linked to the predicted growth of the viscous layer. The boundary-layer displacement thickness distributions for $M_\infty = 0.6$ and 0.875 are shown in Fig. 3. (The experimental data for $M_\infty = 0.875$ were obtained in the Ames 2×2-ft Transonic Wind Tunnel.) Note that different vertical scales have been used for each Mach number. The closure model of Ref. 2, as seen from Fig. 3, predicts the largest displacements of the inviscid flow by the viscous flow. As a result, less pressure recovery along the aft portion of the model and a more forward shock location are predicted. In Fig. 4, the mean-velocity profiles at $x/c = 1$ predicted by the three closure models are compared for $M_\infty = 0.6$ and 0.875.

A Mach contour plot of the solution obtained with the closure model of Ref. 2 at $M_\infty = 0.925$ and a shadowgraph taken in the Ames 6×6-ft Supersonic Wind Tunnel are shown in Fig. 5. Because of the axial symmetry of the flow, in the shadowgraph there appears to be a lambda-type shock structure present, whereas in fact there was only a single shock wave. The illusion of a rear shock is caused from the refraction of light by the single shock in the far field. In both the Mach contour plot and the shadowgraph, the shock is highly curved in the inviscid-flow region. At the model surface, the shock is located at approximately $x/c = 0.65$, whereas far from the model surface it is nearly aligned with the trailing edge. This indeed is a case where a coupled, inviscid-viscous calculation method, based on an outer inviscid-potential solver, would not be expected to give accurate predictions. For the same turbulence-closure model, coupled, inviscid-viscous calculations for the $M_\infty = 0.875$ case[13,14] have resulted in shock positions substantially farther forward (≈ 0.08 chord) than those observed with Navier-Stokes calculations. The reason for this phenomenon is likely the inability of potential methods to describe the rotationality of the flow downstream of the shock wave and the proper shock strength. The sensitivity of coupled, inviscid-viscous

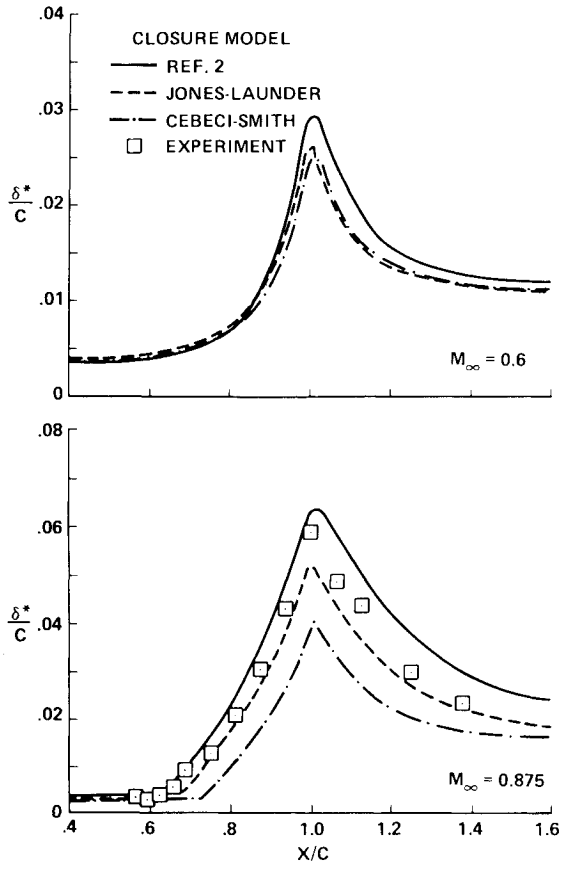

Fig. 3 Predicted boundary-layer displacement thickness distributions for $M_\infty = 0.6$ and 0.875.

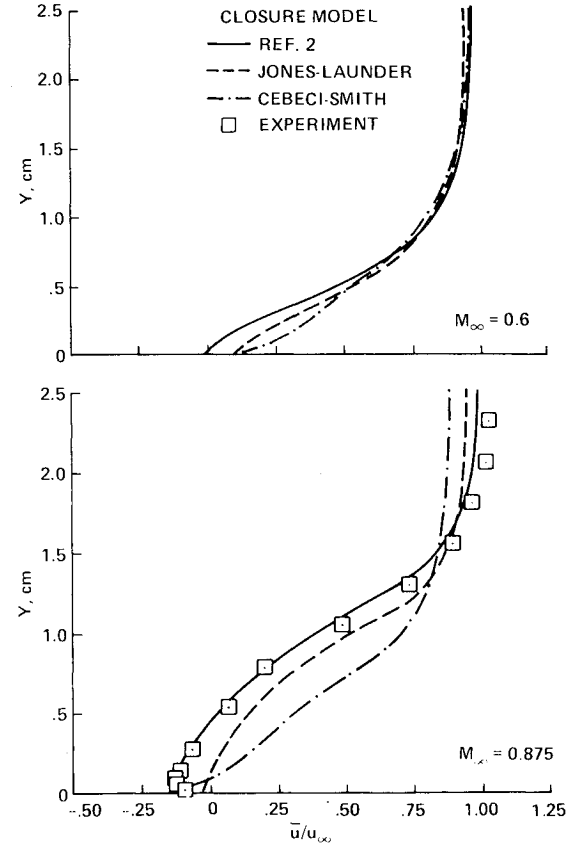

Fig. 4 Predicted, mean-velocity profiles at model trailing edge ($x/c = 1$).

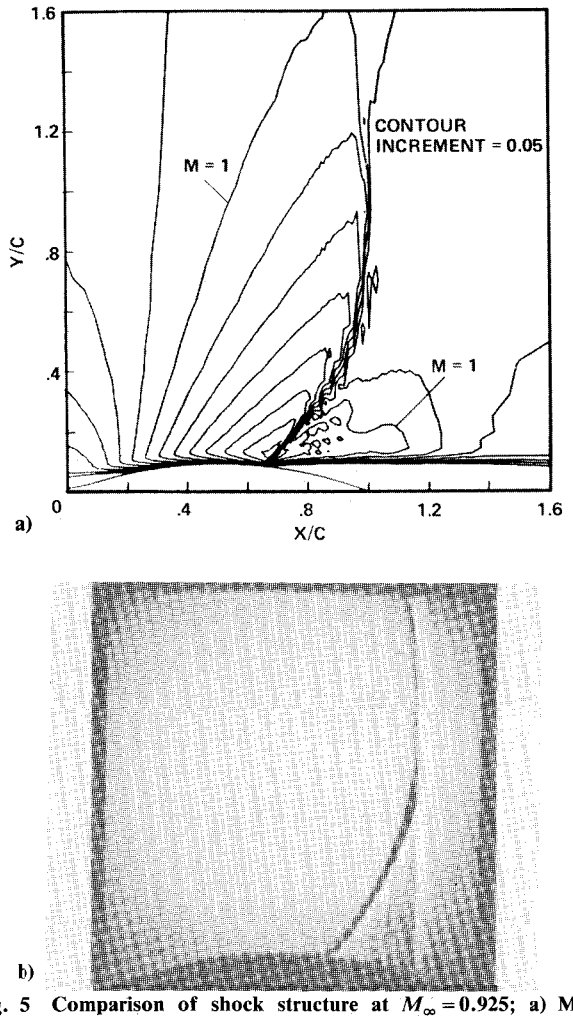

Fig. 5 Comparison of shock structure at $M_\infty = 0.925$; a) Mach contour plot of solution based on model of Ref. 2; b) shadowgraph obtained in Ames 6×6-ft Supersonic Wind Tunnel.

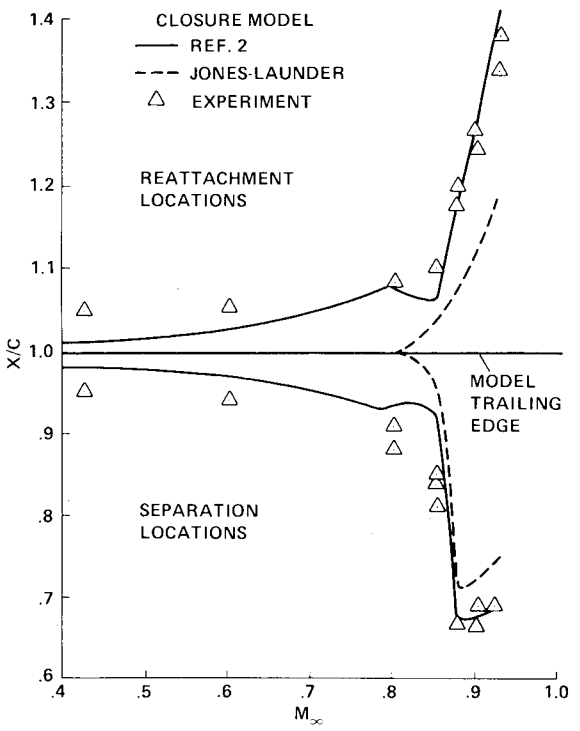

Fig. 6 Comparison of predicted and measured locations of separation and reattachment as a function of freestream Mach number.

methods to the treatment of the shock wave was demonstrated in the airfoil calculations of Ref. 15. In that paper, a significant rearward movement of the shock wave was observed when an approximate correction for entropy losses was applied to the potential equation.

In Fig. 6, the measured (as determined from oilflow visualizations) and predicted extents of separation as a function of freestream Mach numbrs are compared.The closure model of Ref. 2 predicts separation to occur over the entire test range of Mach numbers (0.425 to 0.925). However, the extent of the separation zone is somewhat underestimated at the subcritical Mach numbers. For these Mach numbers, the closure model also slightly overestimates the pressure recovery at the trailing edge, which is consistent with the underprediction of the extent of separation. The overestimation of pressure recovery, however, in small in relation to the results obtained with the Cebeci-Smith and Jones-Launder closure models. Included in Fig. 6 are the predicted extents of separation obtained with the Jones-Launder model. Separtion was not predicted to occur with this closure model until the Mach number exceeded 0.8.

Notice in Fig. 6 that the closure model of Ref. 2 predicts a slight shortening of the separation bubble between $M_\infty = 0.8$ and 0.85. In this Mach number range, the weak shocks resulted in higher Reynolds shear stresses, which enabled the computed boundary layers to better negotiate the strong inviscid-viscous interaction at the trailing edge. Experimental data were not taken between $M_\infty = 0.8$ and 0.85, and so it is not known whether this calculated result is real.

The mean velocity and Reynolds-shear-stress profiles predicted at $M_\infty = 0.875$ with the closure model of Ref. 2 are compared to experimental data obtained in the Ames 2×2-ft Transonic Wind Tunnel (see Fig. 7). In the region between the shock and the trailing edge ($0.69 \le x/c \le 0.94$), the calculated results have been offset 0.03 chord downstream relative to the experimental data to render a more meaningful comparison of the computed and measured results. This distance of 0.03 chord gave the best agreement between the computed and measured mean-velocity profiles in the shock region. It is not clear why an offset equal to the difference in calculated and measured shock position (0.02 chord) did not result in the best agreement. However, in view of the uncertainties in both the calculations and in the experimental data in the shock region, the additional offset of 0.01 chord is considered small. The streamwise locations designated in Fig. 7 correspond to those of the experiment.

In Fig. 7, two sets of experimental results for the Reynolds shear stress are presented. The open symbols correspond to the Reynolds shear stresses as measured in the experiment of Ref. 4 with the x axis horizontal and the y axis vertical. The closed symbols correspond to Reynolds shear stresses obtained by performing a coordinate transformation of these data. In the transformed coordinate system, the x axis is aligned with the direction of the flow at the location where the Reynolds shear stress was a maximum. This coordinate system approximates a shear-layer, aligned coordinate system.

When the flow is highly nonisotropic, as in this case, the measured values of $-\overline{u'v'}$ can depend strongly on the orientation of the measurement coordinate system, as seen from the coordinate transformation equation for $-\overline{u'v'}$:

$$-\overline{u'v'_\theta} = -\overline{u'v'}\cos 2\theta + [(\overline{u'^2} - \overline{v'^2})/2]\sin 2\theta \qquad (12)$$

In the experimental flow, the nonisotropy was significant, causing $(\overline{u'^2} - \overline{v'^2})/2$ to be as large or larger than $-\overline{u'v'}$, whereas in the calculations, this term was always significantly smaller than $-\overline{u'v'}$. This property of the calculations was not unexpected because eddy-viscosity closure models

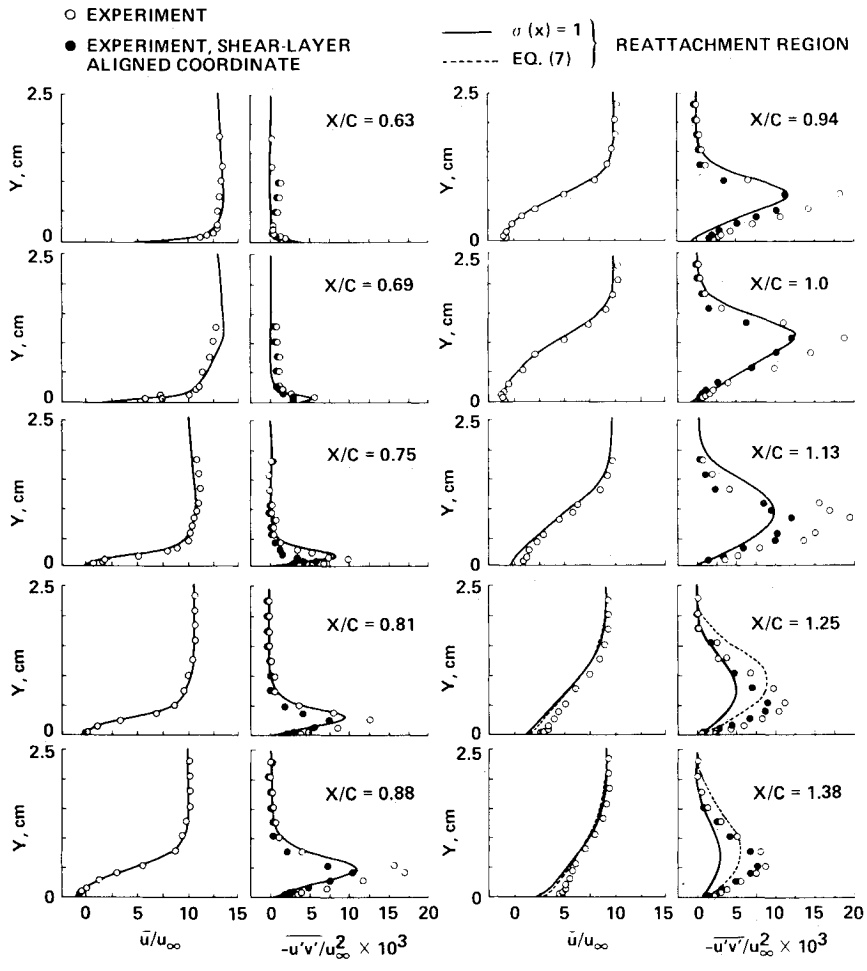

Fig. 7 Comparison of predicted and measured mean-velocity and Reynolds-shear-stress profiles for $M_\infty = 0.875$.

are generally incapable of accurately describing the Reynolds normal stresses. Since the Reynolds normal stresses were not predicted accurately, a realistic comparison of the Reynolds shear stresses cannot be made for any arbitrary coordinate orientation, as seen from Eq. (12). The most meaningful comparison results when shear-layer coordinates are used. In these coordinates, the computed Reynolds shear stresses and normal stresses are a maximum and a minimum, respectively. (The sensitivity of the experimental data to coordinate system orientation *does not* imply the Reynolds normal stresses had a significant effect on the momentum transport.) This point has been overlooked in the comparison of Navier-Stokes calculations with experimental data. In the comparison of boundary-layer calculations to experimental data, the appropriateness of shear-layer coordinates is more obvious. As seen in Fig. 7, the transformation of the data resulted in significant changes in the Reynolds shear stresses, even with a maximum rotation angle of only 10 deg.

There is the danger, however, of overestimating the effects of a coordinate rotation on the Reynolds shear stress by transforming experimental data. This can happen when $\overline{u'^2} - \overline{v'^2}$ is significantly larger than $-\overline{u'v'}$, and the measured values of $\overline{u'^2} - \overline{v'^2}$ are larger than the actual values. Thus, the resultant shear-layer, aligned stresses can be considered reliable only if $\overline{u'^2} - \overline{v'^2}$ were accurately determined in the experiment. This is believed to be the case for the measurement stations at $x/c \geq 0.875$. That the coordinate rotation resulted in maximum correlation coefficients $-R_{uv_\theta}$ of approximately 0.5 (consistent with classic shear-layer measurements) at each of these measurement stations lends supprt to this supposition. For untransformed data, values of $-R_{uv}$ as high as 0.73 were observed at several of these stations. At

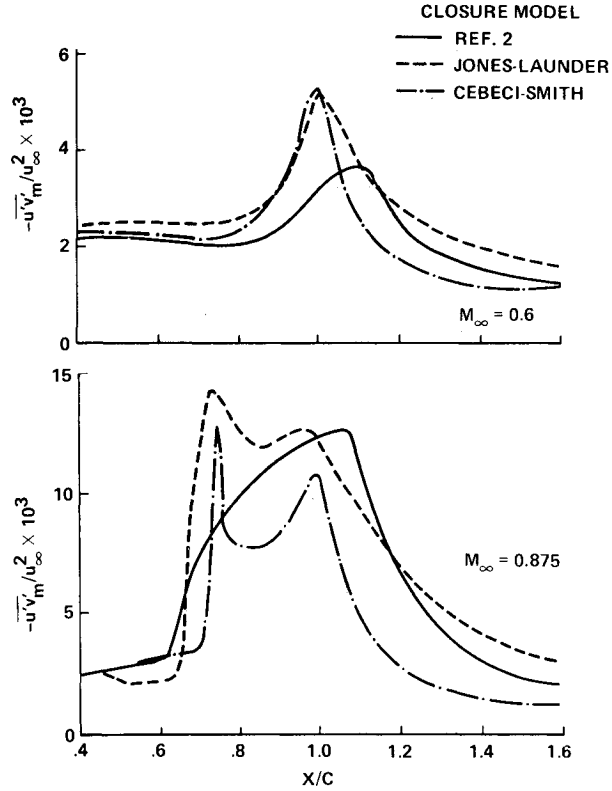

Fig. 8 Predicted variation of maximum Reynolds shear stress with streamwise distance for $M_\infty = 0.6$ and 0.875.

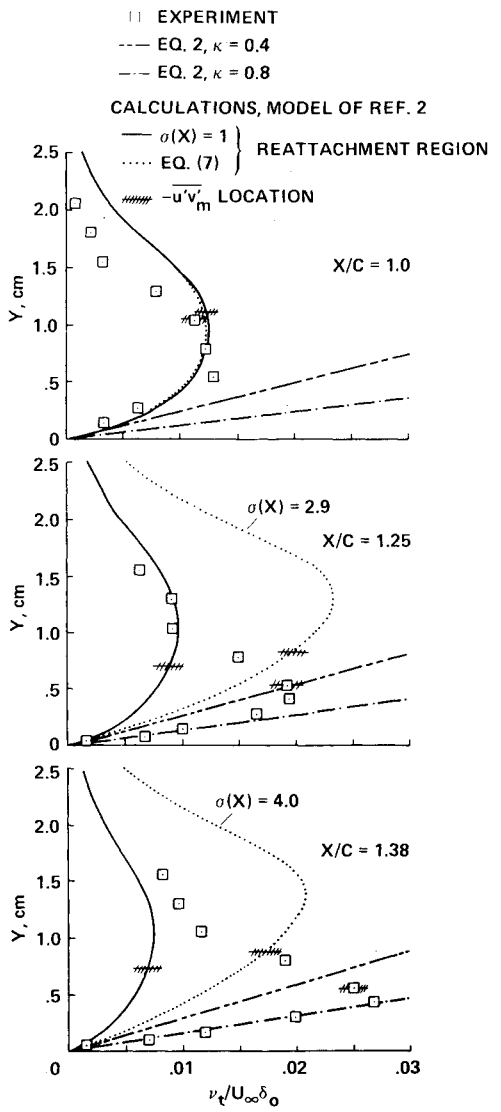

Fig. 9 Turbulent, eddy-viscosity distributions for $M_\infty = 0.875$ at $x/c = 1.0$, 1.25, and 1.38 (reference length $\delta_0 = 1$ cm).

the streamwise stations closer to the shock wave ($x/c = 0.69$, 0.75, and 0.81), where the measurement uncertainties were larger, the changes in $-\overline{u'v'}$ caused by coordinate rotation may have been overestimated. At $x/c = 0.68$, the ratio $(\overline{u'^2} - \overline{v'^2})/-\overline{u'v'}$ measured at the location of maximum Reynolds shear stress was extremely large: 2.5 times larger than that at $x/c \geq 0.875$.

In general, the calculated mean velocities and Reynolds shear stresses are in excellent agreement with the experimental results (the Reynolds shear stresses for a shear-layer, aligned coordinate system). In the region $0.69 \leq x/c \leq 0.81$, the original stresses and those obtained by a coordinate rotation are probably upper and lower bounds, respectively, of the true, shear-layer, aligned stresses. However, the calculations do depart from those of the experiment downstream of reattachment. In the flow reattachment region, the results obtained with $\sigma(x)$ allowed to exceed unity in this region are also presented; upstream, there were no differences in the two solutions. Although larger Reynolds shear stresses are predicted at the downstream stations when $\sigma(x)$ was allowed to attain values well above unity, these larger, Reynolds shear stresses had little effect on the recovery rate of the boundary layer downstream of reattachment. It would appear that larger Reynolds shear-stress gradients in the inner portion of the boundary layer are necessary to obtain the same velocity recovery rate as observed in the experiment. In the next section, it is shown that the larger, shear-stress-gradients observed in the experiment are associated with larger eddy viscosities than predicted by Eq. (2).

Discussion

For the strong, inviscid-viscous interaction cases considered in this paper, the closure model of Ref. 2 predicts substantially less rapid rises in the Reynolds shear stresses than either the Cebeci-Smith or the Jones-Launder model. This is illustrated in Fig. 8, where the maximum Reynolds shear stresses predicted by these turbulence-closure models are plotted against streamwise distance. Note that a different vertical scale has been used for each Mach number case.

From Fig. 7, it can be seen that $-\overline{u'v'}_m/y_m$ is a good measure of the shear-stress gradient $\partial - \overline{u'v'}/\partial y$ in the inner part of the boundary layer. The resultant flow development, of course, is extremely sensitive to the values of $\partial - \overline{u'v'}/\partial y$ attained in the inner part of the boundary layer. If $-\overline{u'v'}_m$ in the calculations is predicted to increase too rapidly at the start of the interaction, shear-stress gradients larger than those observed in the experiment will result. As a consequence, the boundary-layer displacement thickness will be less, and the pressure recovery downstream will be higher. The incremental increases in the shear-stress gradient, in general, will be larger than that of $-\overline{u'v'}_m$, since the larger values of $-\overline{u'v'}_m$ will tend to reduce y_m. With this in mind, the reason for the differences or the similarities (the Jones-Launder and Cebeci-Smith solutions at $M_\infty = 0.6$) in the surface-pressure and boundary-layer displacement thickness distributions predicted by the three closure models becomes obvious after examining Fig. 8. In the regions of increasing maximum Reynolds shear stress, y_m was always observed to be smaller for the Jones-Launder and Cebeci-Smith models. Especially striking in Fig. 8 is the extremely rapid rise in $-\overline{u'v'}_m$ predicted by the Cebeci-Smith model in the shock region.

If there is a weakness in the closure model of Ref. 2, it is in the region downstream of flow reattachment ($x/c \geq 1.17$ for $M_\infty = 0.875$), where, based on the experimental data, the flow recovery is underestimated (see Fig. 7). Fortunately, the departures from the experimental data occur in a region where the boundary-layer displacement effects are sufficiently small that the underestimations of the boundary-layer recovery rate do not influence the prediction of surface pressure. The results, however, do indicate a better characterization is needed of the turbulent-flow behavior near the downstream of reattachment.

In Fig. 9, the predicted eddy-viscosity distributions (for both treatments of the turbulent diffusion downstream of the trailing edge) are compared to the experimental data at $x/c = 1.0$, 1.25, and 1.38. Included in this figure are plots of Eq. (2) based on measured values of $-\overline{u'v'}_m$ and on Kármán constants of 0.4 and 0.8. Evident from this figure is the fact that Eq. (2), with $\kappa = 0.4$, although representing the data well at $x/c = 1.0$, underestimates the measured eddy viscosities in the inner part of the boundary layer at the stations downstream of reattachment.

The underestimation of the eddy viscosities in the inner part of the boundary layer must account for at least some of the underestimation in velocity recovery downstream of reattachment. It definitely explains why the very slow decay of $-\overline{u'v'}_m$ observed in the experiment could not be reproduced by increases in $\sigma(x)$. For example, at $x/c = 1.38$, where $\sigma(x)$ has been limited to a value of 4.0, further increases in $\sigma(x)$ would have little effect on the calculated value of $-\overline{u'v'}_m$, since, at this station, the eddy viscosity at y_m is primarily determined by Eq. (2). The locations of y_m in the calculations and in the experiment are indicated in Fig. 9.

To exactly reproduce the results of this particular experiment downstream of reattachment, some adjustments would have to be made to Eq. (2) for the reattachment region. However, data in addition to those obtained in Ref. 4 need

to be examined to see if, in fact, the eddy-viscosity behavior exhibited by the data of Fig. 9 is observed for reattaching flows in general. It should be noted that the prediction of extremely large values of $\sigma(x)$ occurs only when the flow has undergone massive separation upstream. At $M_\infty = 0.6$, for example, where the separation was less massive, $\sigma(x)$ was observed to achieve a maximum value of 2.8 at $x/c = 1.6$ and then asymptotically approach 1.0 at $x/c = 2.5$.

The closure model of Ref. 2 indicates to its user when problems occur in describing the shear stresses downstream of a massive flow separation region by predicting unreasonably high values of $\sigma(x)$. A better representation for the length scale in Eq. (2) should alleviate these difficulties. However, in the interim, the question arises as to which procedure should be used in this region. The author suggests that Eq. (7) be used but that a conservatively low bound be placed on $\sigma(x)$, say 3.0. Very large values of $\sigma(x)$ could result in an overestimation of the boundary-layer thickness and, as a consequence, in a deterioration in the accuracy of the results.

Before closing, it should be mentioned that Viegas et al.[16] did obtain a substantial improvement over the Jones-Launder integration to the wall results presented in this paper for $M_\infty = 0.875$ using a wall-function approach. They were not entirely satisfied with their solution because of suspected numerical problems around the separation point, but their approach does show promise. A detailed comparison of the present results with solutions obtained by the modeling approach of Ref. 16 over a wide Mach number range could be very informative.

Concluding Remarks

Despite the recognized inadequacies of equilibrium algebraic, eddy-viscosity models in treating strong inviscid-viscous interactions, their use in time-marching, compressible, Navier-Stokes calculations has continued because of the lack of a viable alternative. Two-equation, eddy-viscosity models can provide some improvement in predictive accuracy. The numerical disadvantages of these closure models, however, appear to outweigh these improvements, since there has been reluctance among computational aerodynamicists to use these models. In contrast, the closure model evaluated in this paper is essentially as easy to incorporate into a time-marching, Navier-Stokes method as an equilibrium, algebraic eddy-viscosity model. Yet, as demonstrated, this closure model can provide quite accurate predictions for strong, transonic, inviscid-viscous interactions. This study suggests that the current range of applicability of Reynolds-averaged compressible Navier-Stokes methods can be significantly extended without compromising numerical efficiency.

References

[1]Horstmann, C. C. and Johnson, D. A., "Prediction of Transonic Separated Flows," *AIAA Journal*, Vol. 22, July 1984, pp. 1001–1003.

[2]Johnson, D. A. and King, L. S., "A Mathematically Simple Turbulence Closure Model for Attached and Separated Turbulent Boundary Layers," *AIAA Journal*, Vol. 23, Nov. 1985, pp. 1684–1692.

[3]MacCormack, R. W., "A Numerical Method for Solving the Equations of Compressible Viscous Flow," *AIAA Journal*, Vol. 20, Sept. 1982, pp. 1275–1281.

[4]Bachalo, W. D. and Johnson, D. A., "Transonic Turbulent Boundary-Layer Separation Generated on an Axisymmetric Flow Model," *AIAA Journal*, Vol. 24, March 1986, pp. 437–443.

[5]King, L. S. and Johnson, D. A., "Separated Transonic Airfoil Calculations with a Nonequilibrium Turbulence Model," NASA TM-86830, 1985.

[6]Visbal, M. and Knight, D., "The Baldwin-Lomax Turbulence Model for Two-Dimensional Shock Wave/Boundary-Layer Interactions," *AIAA Journal*, Vol. 22, July 1984, pp. 921–928.

[7]Bradshaw, P., Ferriss, D. H., and Atwell, N. P., "Calculations of Boundary-Layer Development Using the Turbulent Energy Equation," *Journal of Fluid Mechanics*, Vol. 28, Pt. 3, 1967, pp. 593–616.

[8]McDonald, H., "The Departure from Equilibrium of Turbulent Boundary Layers," *Aeronautical Quarterly*, Vol. 19, Feb. 1968, pp. 1–19.

[9]Green, J. E., Weeks, D. J., and Brooman, J. W. F., "Prediction of Turbulent Boundary Layer and Wakes in Compressible Flow by a Lag-Entrainment Method," ARC R&M 3791, 1977.

[10]Cebeci, T. and Smith, A. M. O., *Analysis for Turbulent Boundary Layers*, Academic Press, New York, 1974.

[11]Jones, W. P. and Launder, B. E., "The Prediction of Laminarization with a Two-Equation Model of Turbulence," *International Journal of Heat Transfer*, Vol. 15, Feb. 1972, pp. 301–314.

[12]Kline, S. J., Cantwell, B. J., and Lilley, G. M. (eds.), *The 1980–1981 AFSOR/-HTTM-Stanford Conference on Complex Turbulent Flows: Comparison of Computation and Experiment*, Vol. III, Stanford Univ., Stanford, CA, 1982, pp. 1326–1336.

[13]Carter, J. E., "Viscous-Inviscid Interaction Analysis of Transonic Turbulent Separated Flow," AIAA Paper 81-1241, 1981.

[14]Lee, D. S. and Pletcher, R. H., "Application of a Viscous-Inviscid Interaction Method to Predict Transonic Separated Flows," Third Symposium on Numerical and Physical Aspects of Aerodynamic Flows, California State Univ., Long Beach, Jan. 1985.

[15]Melnik, R. E. and Brook, J. W., "The Computation of Viscid/Inviscid Interaction on Airfoils with Separated Flow," Third Symposium on Numerical and Physical Aspects of Aerodynamic Flows, California State Univ., Long Beach, Jan. 1985.

[16]Viegas, J. R., Rubesin, M. W., and Horstmann, C. C., "On the Use of Wall Functions as Boundary Conditions for Two-Dimensional Separated Compressible Flows," AIAA Paper 85-0180, Jan. 1985.